UC Berkeley
Indoor Environmental Quality (IEQ)

Title

Smart detection of indoor occupant thermal state via infrared thermography, computer vision, and machine learning

Permalink

https://escholarship.org/uc/item/3c9036vz

Journal

Building and Environment, 228(15)

Authors

He, Yingdong
Zhang, Hui
Arens, Edward
et al.

Publication Date

2023-01-30

Copyright Information

Peer reviewed

Smart detection of indoor occupant thermal state via infrared thermography, computer vision, and machine learning

Yingdong He[1], Hui Zhang[1, *], Edward Arens[1], Alexander Merritt[1], Charlie Huizenga[1], Ronnen Levinson[2], Andy Wang[1], Ali Ghahramani[1], Ana Alvarez-Suarez[3]

[1] Center for the Built Environment (CBE), University of California Berkeley, Berkeley, CA, USA

[2] Heat Island Group, Lawrence Berkeley National Laboratory, Berkeley, CA, USA

[3] MoviTHERM, Irvine, CA, USA

* The corresponding author: zhanghui@berkeley.edu

Abstract: The ability to measure occupants' thermal state in real time will enable major advances in the control of air conditioning systems. This study proposes predicting occupant thermal state by a combination of infrared thermography, computer vision, and machine learning. The approach 1) uses cheek, nose and hand temperatures because they are least subject to blockage by hair, glasses, and clothing; 2) measures the distribution of skin temperatures within geometrically defined sub-areas of the face and hand; and 3) uses temperature *differences* within and between these areas to eliminate the effects of calibration drift that are unavoidable in thermal infrared (TIR) cameras. Two series of tests were conducted, respectively in an outdoor carport and an indoor environmental chamber, collecting a total of 48,422 sets of cheek, nose, and hand skin temperatures using a TIR camera and computer-vision technology, coupled with 715 subjective responses of thermal sensations. To predict occupant thermal state, Random Forest classification models were built using either absolute skin temperatures (the maximum and median temperatures of cheek and hand segments, and the temperature of the central spot on the nose), or intra- and inter-segment temperature differences of cheeks, hands, and nose. These measurements were found to accurately predict occupant thermal state. Using the maximum and median temperatures for cheek and nose, or for cheek and hand, predicts thermal state with an accuracy of 92-96%. Using only the intra- and inter-segment temperature differences from cheek and nose is 83% accurate; adding the hand temperature differences increases the accuracy to 96%.

Keywords: Infrared thermography; Computer vision; Machine learning; Thermal comfort; Prediction model.

1. Introduction

Comfortable and healthy indoor environments are important for occupant wellbeing [1] and productivity [2]. Heating, ventilation, and air conditioning (HVAC) systems are used to maintain indoor temperatures within comfort zone boundaries, such as those specified by ASHRAE Standard 55 [3]. Because of individual differences in gender [4], age [5], thermal experience [6], adaptability [7], and dynamic activities [8], thermostat set-points for a single comfort zone rarely satisfy the comfort requirements of all occupants [9]. In addition, buildings are often overcooled or overheated [10] beyond the comfort zone boundaries, due to HVAC system limitations [11] and operator preconceptions of occupant needs [12]. Integrating a hypothetical real-time detection of occupants' thermal state with automatic control of the building's HVAC system [13] might allow the comfort and wellbeing of indoor occupants to be maximized, and also to save HVAC energy [14]. The HVAC system would adjust indoor temperatures according to actual occupant thermal states rather than to keep them presumed set-points.

Skin temperature is correlated with occupant thermal state, as perceived in terms of thermal sensation or thermal comfort. A series of studies of Zhang et al. ([15], [16], and [17]) have created a model of subjective perceptions as a function of local body skin temperatures. They also found that skin temperatures of some body regions (e.g., hand, nose) vary considerably under different thermal conditions while other regions (e.g., forehead, neck) remain relatively stable.

Skin temperatures in such studies were typically measured with contact sensors, such as thermocouples taped to the skin. Such sensing would be inconvenient for controlling HVAC thermostats over time. Likewise, subjective measurement of thermal states, such as having occupants respond to surveys, may not be practical as a mode of control since occupants are distracted by frequent questioning.

Radiometric detection of skin temperatures using infrared thermography could provide a non-disruptive way of monitoring indoor occupant thermal state [18]. This has attracted the attention of researchers in recent years. Most work so far has been in developing models of thermal state from facial skin temperature, because these are most readily captured by thermal infrared (TIR) cameras. De Oliveira et al. [19] correlated TIR camera measurements of cheek, forehead, nose, and periorbital skin temperatures with facial physiological responses like heart rate, facial blood flow, and respiration. Ghahramani et al. [20] developed a method using eyeglass-mounted TIR sensors that measured four facial points: the nose, forehead, cheek, and ear; and they explored how these local skin temperatures varied with different indoor air temperatures. Wang et al. [21] used a TIR camera to measure the upper body temperatures of a subject and directly control the indoor set-point temperature. Faridah et al. [22] used skin temperatures of the forehead, nose, cheek, and chin of 17 male subjects in an artificial neural network to predict their thermal states, reaching a highest accuracy (on a seven-point scale) of 69%. Li et al. [23] used TIR cameras to measure skin temperature at six local body parts (the forehead, nose, cheeks, ears, mouth, and neck), predicting the thermal sensations of 12 subjects with an average accuracy of 85%. Li and

Chen [24] used the mean facial temperatures of indoor occupants, coupled with visual-image-classification of their clothing levels; these inputs were combined to predict occupant thermal state. Cosma and Simha [25] went beyond the head region, using a TIR camera to obtain skin or clothing temperatures of the hand (skin), elbow (clothing), shoulder (clothing), chest (clothing), and head (skin) for predicting dynamic thermal sensations, finding that the mean temperatures of these five locations were 33.5, 34.5, and 35.6 °C for cold, neutral, and warm thermal states respectively. Tejador et al. [26] proposed an infrared thermography method to determine thermal comfort of old people from facial temperatures, finding that they felt thermally neutral when skin temperatures of four facial points (at the nose, forehead, cheekbone and chin, respectively) reached 35 °C.

This team has previously developed a comfort predictive model based on TIR-captured skin temperatures across the entire facial region [27] using the Canny edge detection algorithm to extract edges from both the visual and thermal images. The model calculates hot and cold indexes based on the facial skin temperatures, which are then used as inputs to develop comfort predictive models using machine learning. The hot index is the median temperature of the 10 hottest points on the subject's face, and the cold index is the median temperature of the 5 coldest points on the subject's face. When people are cold, the nose is coldest area of the face; thus the cold index uses points from the nose. Because the nose area is much smaller than the face, a smaller number of points from nose is available for selection. Two potential difficulties with the method involve: 1) the indices' hottest and coldest data points shift as the relative areas of the face are obstructed by presence of eyeglasses, shifting hair and changes to viewing angle; 2) reliance on absolute temperature measurements is subject to drifts in TIR calibration [28].

The above studies suggest that infrared thermography might provide an effective way of monitoring and predicting indoor occupant thermal state for automated HVAC control. However, some critical issues remain to be addressed:

(1) First, the selected local body parts in the existing studies are not always viewable by TIR cameras in practice. For example, the forehead temperature may be a good index for predicting occupant thermal state [19], but the forehead may be covered by a hat or hair. Similarly ears and necks may be covered by hair or clothes [23].

(2) Our early tests showed that when people were warm, skin temperatures over face and hand were uniform, but when people were cold, there were not only large temperature differences *between* body parts such as cheeks and hands, and also large temperature variations *within* a body part. The intraregional temperature variation within the cheek and hands might usefully contribute to model predictions. For these reasons, obtaining skin temperature distributions over an area of a body segment could have multiple advantages. So far only one model previously developed by this team [27] has measured maximum or median temperatures.

(3) Past studies have typically used skin temperatures at selected local measurement points as inputs for predicting thermal state [22]. Large individual differences in body shapes (e.g., face shapes) can make the location of specific

points challenging. Measurements more closely representing the area surface temperature of a whole local body segment (like the maximum and median temperatures of areas of cheeks or hands) will be more stable than those of selected measurement points.

(4) Finally, TIR cameras suffer systematic errors from parameters such as the user-defined surface emissivity, sensor element efficiency, and the temperature of the sensor [28]. Each of these systematic errors has been difficult to eliminate without adding extra external sensors (e.g., contact thermometers) for real-time calibration. Algorithms are needed that can detect thermal state while overcoming systematic errors of TIR cameras.

Aims: Following from the above, this study was planned to develop an occupant thermal-state predictive approach using statistical (maximum and median) skin temperatures of cheeks and hands, as well as a locationally-defined set of nose temperatures. These skin regions appeared to be most reliably viewed by camera. To overcome the systematic errors of infrared thermography, we also aimed to use only intraregional and interregional *differences* in cheek, hand, and nose temperatures to predict occupant thermal state.

2. Experimental method

2.1 Facility setup

In overview, two series of tests were conducted in an outdoor carport and an environmental chamber, respectively. In total, 48,422 sets of skin temperature data and 845 thermal sensation votes were collected from 20 and 13 subjects in two locations to build and test the Random Forest models.

To establish thermal sensation models based on skin temperatures, we need to perform human subject tests under cool, neutral, and warm environments. Due to University restrictions on conducting indoor experiments during the COVID-19 pandemic, the first part of the tests was carried out outdoors. Tests from December 2020 to May 2021 were carried out in a well-ventilated outdoor carport of a house (Fig. 1a) located in Berkeley, California. We set up a thermal enclosure within the carport using thick fabric curtains serving as four "walls", with large openings at top and bottom. Because it was naturally ventilated in the winter season, the test conditions covered cool and neutral conditions (see Section 2.4). The tests in the carport were mainly conducted from 15:00 to 20:00 local time (LT) with the indoor temperature varying between 12 and 20 °C on different days. Each test continued for one hour. Within the hour, the environmental temperature never varied by more than 2 °C.

The other test site was an indoor temperature-controlled environmental chamber (Fig. 1b) at the Center for the Built Environment (CBE), University of California, Berkeley, in which human subject tests were performed from June to July 2021, covering warm and neutral conditions. The chamber tests were mainly performed from 10:00 to 18:00 LT, and the indoor temperature was maintained at either 24 or 30 °C, depending on the test plan (see Section 2.4).

In both the carport and the chamber, a seat and a small desk with a computer mouse was provided for subjects, and a

pair of cameras (FLIR Blackfly S GigE [29] visual camera and FLIR A315 [30] TIR camera) were placed in front of the

seat (1.6 m horizontal distance and 1.4 m above floor). The rated accuracy of the TIR camera is ±2 °C (within the range

of -20 to 120 °C). A passive temperature reference—a surface of known thermal emittance whose unregulated temperature

is continuously measured with a contact thermometer—was mounted on a table next to the subject. The two cameras were

connected to a laptop computer and provided real-time data collection (see Fig. 1c). The detailed function of the cameras
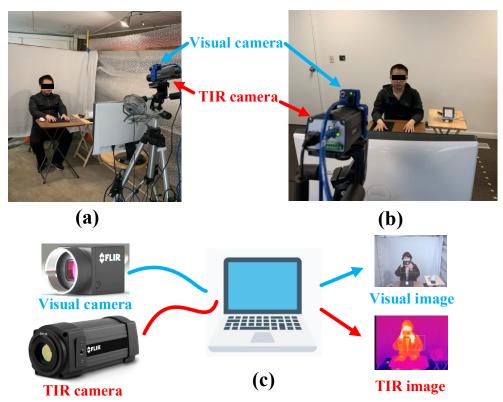
is described in Section 2.2.

Figure 1. The experimental sites: (a) carport, (b) chamber; and (c) coordination of the visual and infrared cameras.

2.2 Skin temperature data generation

The visual camera and TIR camera were used to capture the real-time temperatures of cheeks, noses, and hands. The

procedure of human body detection and skin temperature acquisition is shown in Fig. 2 and illustrated as follows:

(1) Image generation: the visual camera and TIR camera generate visible and TIR images respectively, at the rate of

four visible and four TIR images per second. This step generates original images that will be manipulated to obtain skin

temperature data in the subsequent steps.

(2) Image pre-alignment: each TIR image is rescaled and padded to the same size with the visual image of the same

pair. Through the image pre-alignment, the visible and TIR images are in the same size, which increases the matching

accuracy of human body areas in step (4).

(3) Human body detection: the OpenPose package [31] is used to detect the human body within the field of the view

of the visual images.

(4) Visible-to-thermal image registration: the OpenCV library [32] is used to detect Canny edges and then match the human body in the visual and TIR images.

(5) Key point detection and area determination for cheeks and hands: the key points on the detected human body for locating cheek and hand areas (both left and right) are extracted to formulate enclosed areas which are then located in the TIR images. Each area contains about 100 pixels of TIR image, with each pixel comprising one temperature value.

(6) Data extraction: according to the detected key points, statistical temperature and area data from the cheek and hand regions are extracted from the TIR images. For the nose, we used the data from the central point of the nose because it is difficult to define an accurate area for the whole nose. We did not use skin temperature from the forehead because foreheads are often covered by hair.

(7) Data filtration: data from unmatched visual and TIR images, images with failed visible-to-thermal registration, or instances having large sudden temperature changes in one key point are filtered out to increase the accuracy of skin temperature data. After filtration, the rest data are saved.

(8) Modelling: the saved data are used to build machine learning models for predicting occupant thermal states, as elaborated in Section 3 of this paper.
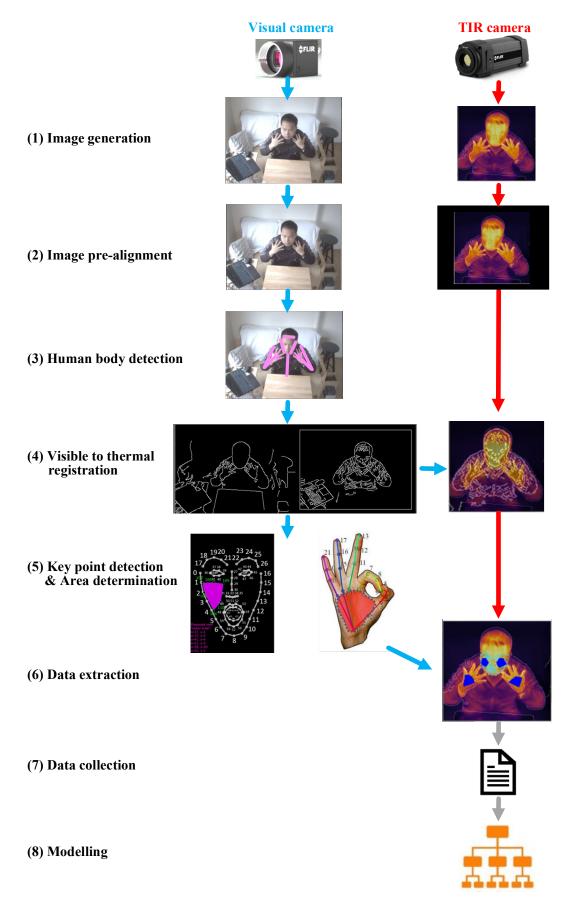
Figure 2. The procedure of thermal state prediction which combines camera imaging, body detection, image registration, data extraction, and modelling.

2.3 Testing procedure

As shown in Fig. 3, each test was 70 minutes, consisting of a 10-min acclimation period and a 60-min testing period. During the acclimation period, the testing procedure and the survey content were described to the subjects. Only one subject was tested at a time, whether in the carport or in the chamber. During the testing period, the subject completed a thermal sensation survey every five minutes, totaling 13 surveys; the grey triangles in Fig. 3 mark the time points of the surveys. The thermal sensation survey has a continuous scale from "very cold" (–4) to "very hot" (+4) (Fig. 3b). Subjects were asked to select the level that most properly represented their thermal sensations, which are classified into three categories (warm, neutral, and cool) for modelling (further clarified in Section 3.1). During the testing period (60-min), the subjects were watching videos (e.g., TV shows, movies, and nature documentaries) played on a screen near the TIR camera. The videos contained no information related to the research content of this study. In total, 845 subjective sensation votes were collected from 20 individual subjects in the carport and 13 individual subjects in the chamber.
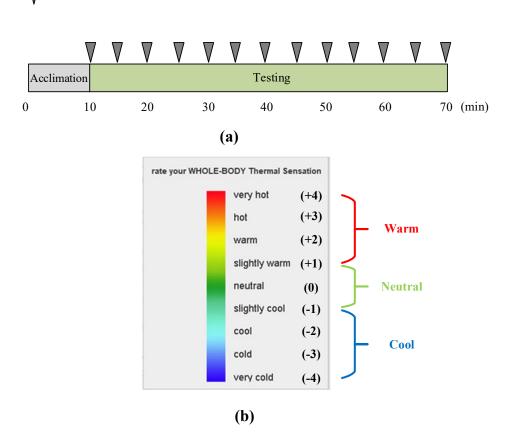

(a)

(b)

Figure 3. (a) The testing procedure and (b) the used questionnaire.

2.4 Test conditions and subjects

As shown in Table 1, the cool tests were performed in the carport, and the warm tests were performed in the environmental chamber, while neutral tests were performed at both testing locations. For the carport tests, 20 subjects (13

males and 7 females) were recruited to participate in both the cool and the neutral tests. For the chamber tests, 14 subjects (11 males and 3 females) were recruited, of whom 11 participated in both warm and neutral tests, 2 participated in only the warm tests and one participated in only the neutral tests. The tests in the carport and the chamber had different subjects and imbalanced sex ratios because recruitment was difficult during the COVID emergency and comparison of gender differences was not an objective of the study.

The subjects did not know the purpose of the study. They were healthy while participating, and did not drink alcohol or smoke on the day of testing.

Table 1. Environmental conditions and subject characteristics for trials conducted in the unconditioned carport and the conditioned environmental chamber.

Location	Ambient air temperature (°C)	Condition	Subject information			
			Count[1]	Age (y)[2]	Height (cm)[2]	Weight (kg)[2]
Carport (unconditioned)	11-20	Cool[3]	20 (13, 7)	31.0 ± 14.7	172.5 ± 9.5	66.2 ± 10.3
Carport (unconditioned)	11-21	Neutral[4]	20 (13, 7)	31.0 ± 14.7	172.5 ± 9.5	66.2 ± 10.3
Chamber (conditioned)	24	Neutral[5]	12 (9, 3)	37.0 ± 11.7	171.1 ± 8.0	67.2 ± 11.7
Chamber (conditioned)	30	Warm[5]	13 (10, 3)	40.5 ± 15.7	172.2 ± 8.2	68.4 ± 11.8

[1] Total (male, female).

[2] Mean value ± standard deviation.

[3] Each subject wore a long-sleeved shirt, sweater, trousers, socks, and shoes.

[4] Each subject wore a heavy jacket, long-sleeved shirt, sweater, trousers, socks, and shoes.

[5] Each subject wore a long-sleeved shirt, trousers, socks, and shoes.

3. Machine learning model

3.1 Data for developing machine learning models

To reduce the effects of subjects' thermal states prior to the acclimation period, the data collected in the last 50 minutes were used, when subjects' thermal sensations had become stable. In total, 48,422 sets of skin temperatures and 715 sensation votes were used to build predictive models. Each set includes the skin temperatures of the nose and two regions (cheeks and hands) shown in Fig. 2. For each cheek or hand region, three temperature statistics were extracted: the maximum temperature, the median temperature, and the minimum temperature. For the models that we describe below, we used the maximum and the median temperatures of the cheek and hand regions, since these two statistics are less affected than is the minimum temperature by the possible presence of a partially covering object. Assuming that subjects had symmetrical skin temperatures on both sides of the body, regions (cheeks and hands) on the left side were selected for analysis.

The algorithm of body segment recognition could detect relatively large and stable body parts like face and the back of the hand, but was less reliable for detecting finger location. We therefore used the temperature of the back of the hand for

the models described in this paper. We are now investigating a new algorithm capable of detecting finger temperatures but this will be presented in a future report.

Thermal sensation votes reported on a scale of -4 (very cold) to +4 (very hot) were simplified to "warm", "cool", or "neutral" sensations (see Fig. 3b) for data analysis. We mapped votes higher than +1 (slightly warm) to warm, votes lower than –1 (slightly cool) to cool, and votes between –1 and +1 (inclusive) as neutral. Skin temperatures were recorded at a rate of 4 Hz, while votes were collected every 5 minutes. The temperatures were then matched with the votes as follows: during the last 50 minutes of each test, if two consecutive votes indicate the same thermal sensation (warm, cool, or neutral), then that thermal sensation was assigned to all skin temperatures collected within the time period between the two votes (inclusive). The number of pairs of thermal states and skin temperatures was thereby increased for conducting machine learning. This algorithm for assigning thermal sensations to skin temperature measures yielded 19,341 warm, 10,671 cool, and 18,410 neutral skin temperature/sensation pairs.

Moreover, to reduce the sample imbalance among the warm, cool, and neutral data, the cool and neutral data were oversampled by machine learning in a randomized approach to the same size of the warm data (19,341). This increased the size of the total dataset to 58,023. The Synthetic Minority Oversampling Technique (SMOTE) first picks a random sample (called Sample A) of the minority classification (cool or neutral); then, several (usually five) neighbor data samples of the same classification are located, and one of the neighbor samples is selected (called Sample B);, a new data sample is then generated at a randomly selected point between Samples A and B in feature space. Through repeating these steps, the data of the minority classifications (cool and neutral data) are oversampled until they reach the same size as the warm data. The details of SMOTE can be seen in [33].

3.2 Model selection

The Random Forest model [34], a non-parametric data-driven method to address regression or classification problems, was adopted to model thermal states. Compared with other data-driven methods, the Random Forest model is characterized by high accuracy, fast solutions on large datasets, the ability to estimate relative importance of features before models are built, and favorable user-friendliness without requiring users to optimize model parameters. It also does not require complex parametric optimization.

In this study, the Random Forest model was built by using the scikit-learn package [35] with Python language. Two critical model parameters, the estimator number (the number of decision trees) and the maximum depth (the maximum node number of decision trees), were set at 400 and 10, respectively. Other parameters were set at the default levels defined by the scikit-learn package.

3.3 Feature selection

The model "features" (inputs) selected include the nose temperature, the maximum cheek temperature, the median

cheek temperature, the maximum hand temperature, and the median hand temperature. A feature importance analysis was performed by the Random Forest algorithm to identify the importance levels of model inputs (see Section 4.2). The higher the value, the more importance in affecting the output.

3.4 Model performance evaluation and validation

The entire dataset was randomly divided into a training dataset (80%) and a testing dataset (20%). We report model accuracy as the fraction of correctly predicted sensations in the testing dataset. The final models obtained in this study were also used to predict the thermal sensations previously observed in two studies by authors of this paper: a field study [4] and a lab study [36]. In these validations, the cheek and hand temperatures of studies [4] and [36], which were measured by thermocouples, were input to the built models; our model's predictions were compared to the sensation votes reported in each study after reclassifying these votes as warm, cool, or neutral following the method mentioned in Section 3.1 (with the reference to Fig. 3b). The detailed validation is presented in Section 4.4.

4. Results

4.1 Data overview

Fig. 4 shows the skin temperature distribution for different thermal states. The main finding is that the cheek skin temperature varies less under cool and neutral sensations than the nose and hand skin temperatures. Under warm sensations, the changes for cheek, nose, and hand are small and similar.

For example, the maximum cheek temperatures were 30-35, 32-36, and 35-37 °C (spans 5, 4, and 2 °C) when the subjects were cool, neutral, and warm, respectively, while the median cheek temperatures were 28-33, 30-35, and 35-37 °C (spans 5, 5, and 2 °C) when the subjects were cool, neutral, and warm, respectively. The nose temperatures were 22-30, 30-36, and 35-37 °C (spans 8, 6, and 2 °C) in cool, neutral, and warm conditions. The maximum hand temperatures were mainly 18-30, 30-36, and 35-37 °C (spans 12, 6, and 2 °C) when the subjects were cool, neutral, and warm; the median hand temperatures were mainly 15-30, 28-35, and 34-37 °C (spans 15, 7, and 3 °C) correspondingly. The hand temperatures were lower than the nose temperatures when the subject reported a cool sensation. For all three segments, the skin temperature variations were greater for the cool and neutral sensations than for the warm sensation. For hands or cheeks, the temperature difference between the maximum and the median decreased from 3-4 °C to 1.0-1.5 °C as the subjects switched from cool sensation to warm sensation. The larger variations of hand temperature in cool conditions seen in Fig. 4 is due to the greater vasoconstriction/dilation in body extremities than head.

Fig. 5 shows the temperature differences among different body segments in cool, neutral, and warm conditions. When subjects felt cool, temperature differences between cheek and nose (Cheek_max – Nose, in Fig. 5) or between cheek and hand (Cheek_max – Hand_max, in Fig. 5) were typically 2-10 and 0-10 °C, respectively; when subjects felt neutral or warm, the corresponding temperature differences were 0-5 °C and 0-2 °C respectively. The different responses of the

cheek, nose, and hand temperatures to the different thermal sensations (shown in Figs. 4 and 5) make it possible to predict thermal sensation using either the absolute temperatures, or the temperature differences between different body segments, or temperature variations among single body segments.
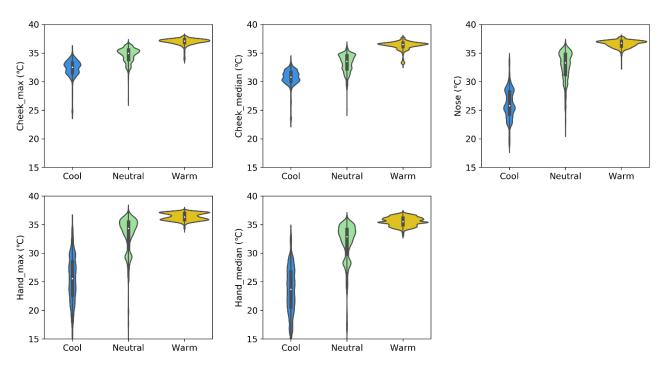

Figure 4. Distributions of local skin temperatures. Cheek_max is the maximum temperature of the cheek region; Cheek_median is the median temperature of the cheek region; Nose is the central spot temperature of the nose; Hand_max is the maximum temperature of the hand region; Hand_median is the median temperature of the hand region.
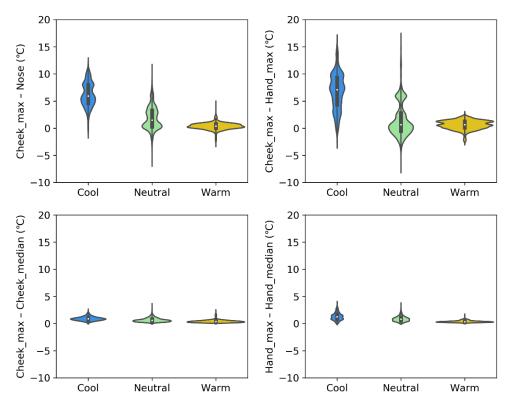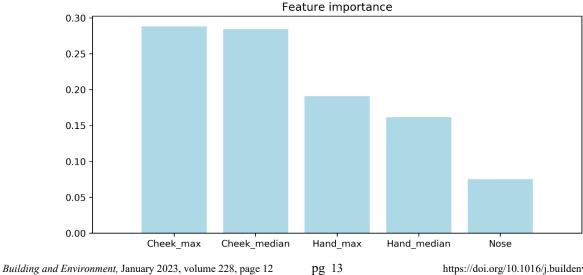
Figure 5. Distributions of skin temperature *differences*. Cheek_max is the maximum temperature of the cheek region; Cheek_median is the median temperature of the cheek region; Nose is the central spot temperature of the nose; Hand_max is the maximum temperature of the hand region; Hand_median is the median temperature of the hand region.

4.2 Feature importance

Fig. 6 illustrates the feature importance of the selected variables. The most important variable is the maximum cheek temperature, followed by the median cheek temperature, maximum hand temperature, the median hand temperature, and finally the nose temperature. Thus, when establishing the models described in Section 4.3, cheek temperatures were used as the main features. All models except one include the maximum or medium temperatures from the cheek. The models use either absolute temperatures or temperature differences, as described in Section 4.3.

Figure 6. Importance of the selected temperature features. Cheek_max is the maximum temperature of the cheek region; Cheek_median is the median temperature of the cheek region; Nose is the central spot temperature of the nose; Hand_max is the maximum temperature of the hand region; Hand_median is the median temperature of the hand region.

4.3 Model performance

4.3.1 Model performance with absolute temperatures

Table 2 shows the model performance of the testing dataset with absolute temperatures of different body segments. Using statistical temperatures of a single region (the maximum and median temperatures of cheeks or hands as selected features) predicts thermal sensation with 86% to 88% accuracy (Models 1 and 2). Adding the nose temperature to the cheek temperatures (Models 3-5) increases the model accuracy to 91.9-96.3%, while adding the hand skin temperature to the cheek temperatures (Models 6 and 7) raises it to 93-95%. Using cheek, nose, and hand temperatures as model features simultaneously gives the highest accuracy, up to 99%. It should be noted that using the pair of cheek and nose temperatures or the pair of cheek and hand temperatures both achieved high accuracy, which indicates that measuring skin temperatures of only two body segments among these three is enough to accurately predict thermal sensations. This finding is consistent with that of Dai et al. [37], where skin temperatures of any two body parts could accurately represent thermal states.

Table 2. Model accuracy with different combinations of local skin temperatures.

ID	Features[1]	Size of testing dataset	Accuracy	Reported state	Predicted state		
					Cool	Neutral	Warm
Model 1	Cheek_max	11,605	0.879	Cool	3,379	475	4
	Cheek_median			Neutral	593	3,132	151
				Warm	6	171	3,694
Model 2	Hand_max	11,605	0.863	Cool	3,623	235	0
	Hand_median			Neutral	348	2,954	574
				Warm	0	430	3,441
Model 3	Cheek_max	11,605	0.919	Cool	3,595	263	0
	Nose			Neutral	319	3,380	177
				Warm	0	183	3,688
Model 4	Cheek_median	11,605	0.941	Cool	3,636	222	0
	Nose			Neutral	300	3,501	75
				Warm	0	90	3,781
Model 5	Cheek_max	11,605	0.963	Cool	3,730	128	0
	Cheek_median			Neutral	210	3,628	38
	Nose			Warm	0	51	3,788
Model 6	Cheek_max	11,605	0.931	Cool	3,677	181	0
	Hand_max			Neutral	253	3,458	165
				Warm	0	196	3,675
Model 7	Cheek_median	11,605	0.956	Cool	3,729	129	0
	Hand_median			Neutral	238	3,569	69

				Warm	0	78	3,793
Model 8	Cheek_max	11,605	0.966	Cool	3,780	78	0
	Nose			Neutral	117	3,667	92
	Hand_max			Warm	0	108	3,763
Model 9	Cheek_median	11,605	0.982	Cool	3,805	53	0
	Nose			Neutral	100	3,752	24
	Hand_median			Warm	0	29	3,842
Model 10	Cheek_max	11,605	0.990	Cool	3,815	43	0
	Cheek_median			Neutral	46	3,814	16
	Nose			Warm	0	12	3,859
	Hand_max						
	Hand_median						

[1] Cheek_max is the maximum temperature of the cheek region; Cheek_median is the median temperature of the cheek region; Nose is the central spot temperature of the nose; Hand_max is the maximum temperature of the hand region; Hand_median is the median temperature of the hand region.

4.3.2 Model performance with intra- and inter-segment temperature *differences*

Most TIR cameras have a "drift" issue [38], in which all readings from the pixel array suddenly change 1-2 °C. To receive correct absolute temperatures requires complicated data correction [39] sometimes involving an external device of known temperature. A way to cope with such drift is to use a model that only inputs skin temperature *differences* since drift does not affect the temperature differences from the pixel array. The differences can be intra-segment (difference within one body segment—e.g., hand) or inter-segment (difference between two different body segments—e.g., cheek and hand). Since cheek temperatures have larger importance (see Fig. 6) and higher prediction accuracy (see Table 2) than hands and nose, the models using temperature differences only always include temperature differences that incorporate either the maximum or median temperature of the cheek. Table 3 shows the model performance of the testing dataset using only intra-segment and inter-segment temperature differences. Using intra-segment temperature differences only (within-cheek or within-hand temperature differences) has lower accuracy (71%) (Model 11) than using statistical temperatures of a single region (Models 1 and 2). Using inter-segment temperature differences (temperature differences between cheek and nose and between cheek and hand) provides prediction accuracy around 80% (Models 12 and 13). When intra-cheek temperature difference and inter-segment temperature differences (cheek and nose, cheek and hand) are used, the accuracy is 92% (Model 15). If intra-cheek, intra-hand, and inter-segment temperature differences (cheek and nose, cheek and hand) are used simultaneously, the model accuracy reaches 96% (Models 16). Comparing Models 13 (facial skin temperatures only) and 16 (facial and hand skin temperatures) shows that adding hand skin temperature increases the model accuracy by 13 percentage points, from 83% in Model 13 to 96% in Model 16.

Table 3. Model accuracy with different combinations of skin temperature differences.

ID	Features[1]	Size of testing dataset	Accuracy	Reported state	Predicted state		
					Cool	Neutral	Warm
Model 11	Cheek_max – Cheek_median	11,605	0.709	Cool	2,924	811	123
	Hand_max – Hand_median			Neutral	1,004	2,182	690
				Warm	128	618	3,125
Model 12	Cheek_max – Nose	11,605	0.828	Cool	3,545	307	6
	Cheek_max – Hand_max			Neutral	321	2,777	778
				Warm	4	581	3,286
Model 13	Cheek_max – Cheek_median	11,605	0.830	Cool	3,466	384	8
	Cheek_max – Nose			Neutral	526	2,788	562
				Warm	8	481	3,382
Model 14	Cheek_max – Cheek_median	11,605	0.876	Cool	3,549	305	4
	Cheek_max – Nose			Neutral	419	3,075	382
	Hand_max – Hand_median			Warm	2	324	3,545
Model 15	Cheek_max – Cheek_median	11,605	0.923	Cool	3,711	146	1
	Cheek_max – Nose			Neutral	241	3,373	262
	Cheek_max – Hand_max			Warm	1	237	3,633
Model 16	Cheek_max – Cheek_median	11,605	0.959	Cool	3,767	90	1
	Cheek_max – Nose			Neutral	132	3,598	146
	Cheek_max – Hand_max			Warm	1	103	3,767
	Hand_max –Hand_median						

[1] Cheek_max is the maximum temperature of the cheek region; Cheek_median is the median temperature of the cheek region; Nose is the central spot temperature of the nose; Hand_max is the maximum temperature of the hand region; Hand_median is the median temperature of the hand region.

4.4 Further model validation

We tested the model performance using data from two past studies done by some authors of this paper: one field study [4] and one lab study [36]. Fig. 7 shows cheek and hand temperatures obtained from these studies. In the field study, the data were collected from 1,167 students in classrooms, with sample sizes for the cool, neutral, and warm sensations of 902, 261, and 4, respectively. The small number of "warm" sensation was because that the field study was conducted in winter season when the occupants were generally in cool conditions. The cheek temperatures were typically 25-35, 27-36, and 28-37 °C (spans 10, 9, and 9 °C), respectively when the subjects were cool, neutral, and warm, while the hand temperatures were typically 20-32, 25-34, and 27-34 °C (spans 12, 9, and 7 °C) when the subjects were cool, neutral, and warm. In the lab study, performed in an environmental chamber under cool, neutral and warm conditions, the sample sizes of the cool, neutral, and warm sensations are more balanced, reaching 9,447, 7,078, and 5,964, respectively. The data were obtained from 43 participants (each participant experienced multiple test conditions). The cheek temperatures were mainly 26-35, 33-36, and 35-37 °C (spans 9, 3, and 2 °C) when the subjects were respectively cool, neutral, and warm.

Hand temperatures were mainly 22-32, 34-36, and 35-37 °C (spans 10, 2, and 2 °C) when the subjects were respectively cool, neutral, and warm.
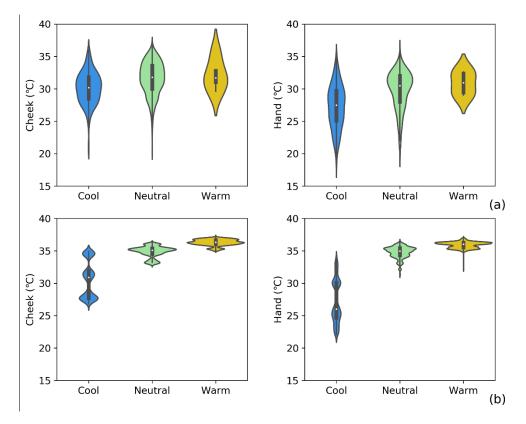

Figure 7. Cheek and hand temperatures of (a) a field [4] and (b) a lab [36] studies.

Table 4 presents the results of model validation using the data from studies [4] and [36]. In these two studies, the cheek and hand temperatures were measured near the center point of cheeks and hands (no nose skin temperature was collected), so the data are used to validate Model 7 which uses the median cheek and hand temperatures as features. In Ref. [4], the skin temperature was obtained using handheld thermocouple sensors touching the skin. In Ref. [36], the skin temperature was monitored by thermocouples taped to the skin with medical tape. As shown in Table 4, the model predicts the results of these two studies with an accuracy around 70% (69% for [4] and 76% for [36]). Deploying a trained machine learning model to predict new people's thermal state in general have an accuracy lower than 60% [37]. The 70% accuracy means that Model 7 is reasonable for predicting the two independent studies, although the accuracy is lower than the 96% accuracy using the testing data of the current study (see Model 7 in Table 2). The lower accuracy can be attributed to three factors. First, the skin temperature data of studies [4] and [36] were only measured at a point on the cheek or hand; they are not regional medians. The inconsistent skin points may be causing unpredictable variations and thus reduce the model accuracy. Second, the contact temperatures obtained from thermocouples in the two earlier studies might differ from the radiometric temperatures obtained from the TIR camera in the current study. Third, there are always individual differences of physiological and psychological responses to ambient environments among different people; the individual differences

would lower the accuracy of the models when applying models developed from one population to another. To increase the accuracy for a particular population, machine learning can be applied to data obtained specifically from that population and then applied to rebuild the models using the featured temperatures presented in Tables 2 and 3 for this population. This is further addressed in the Discussion section.

Table 4. Model 7 validation with the data from studies [4] and [36] (cheek and hand skin temperatures as features).

Study	Input variable	Sample size	Accuracy	Actual state	Predicted state		
					Cool	Neutral	Warm
[4]	Cheek temperature	1,167	0.686	Cool	156	105	0
	Hand temperature			Neutral	247	645	10
				Warm	0	4	0
[36]	Cheek temperature	22,489	0.757	Cool	3,765	2,199	0
	Hand temperature			Neutral	0	4,366	2,712
				Warm	0	557	8,890

5. Discussion

5.1 Significance and applications

(1) This study proposes a new approach to detecting occupant thermal state using a combination of visual and TIR cameras, and skin temperature data from discrete regions of the face and hands. Distinct from previous studies that used skin temperatures of selected points or the average of an area to represent local body parts, the method proposed in this study employs the maximum and median skin temperatures from highly sampled cheek and hand segments. The intraregional temperature variation within the cheek and hands contributes to the model predictions; the variations are larger when feeling cool and smaller when feeling warm. For these reasons, obtaining skin temperatures over a defined sub-area of a body segment has multiple advantages.

(2) The intra- and inter- temperature difference models (presented in Table 3) provide a practical way to reduce systematic temperature deviations of TIR cameras without the use of external calibration to correct TIR cameras measurements. It also makes it possible to detect occupant thermal state using low-cost TIR cameras of a relatively lower accuracy: inexpensive TIR cameras may report temperature differences within a scene with sufficient accuracy even if their absolute temperature values have low accuracy.

(3) Although the built models were generated by using images of a limited number of subjects (20 subjects in the carport and 13 in the chamber), they still well-predict thermal sensations reported in a past field study (1,167 subjects) and a past lab study (43 subjects), with an accuracy around 70%. If the dataset for building these machine learning models were extended by adding actual personalized data as might be obtained within real buildings, the model performance would be improved.

(4) Facial (cheek and nose) skin temperatures have in the past been easier to capture than hand skin temperatures. To evaluate the hand skin temperature contribution to the model prediction accuracies we can look at the models that only use skin temperature differences as examples: in Model 13, using only intra-segment and inter-segment temperature differences from cheeks and nose, the model prediction accuracy was 83%. In Model 15, when the skin temperature difference between cheeks and hands was also incorporated, the model accuracy reached 92%. In Model 16, when intra-segment temperature difference from hands is combined with the inputs of Model 15, the model attained 96% accuracy. Therefore one can choose between simpler models that use only facial temperatures or more accurate models that require both facial and hand temperatures. The various models from this study provide flexibility in predicting occupant thermal states according to the actual availability of local body part temperatures (e.g., sometimes, hands may not be seen by TIR cameras).

5.2 Limitations

The following limitations of this study might guide future work:

(1) The number of subjects of this study was limited due to the pandemic. Future studies should adopt larger sample sizes of subjects to create stronger models.

(2) The subjects were in stable thermal conditions during the testing, similar to extended seated activities in offices and classrooms. In practice occupants often experience dynamic thermal conditions due to changing activity levels in buildings or outdoor-indoor transitions. Whether the models developed here can predict dynamic thermal sensations of occupants who may be moving or changing activity levels is a very interesting topic for future investigations.

(3) The gender ratio is not balanced in this study. Females may have different thermal responses to ambient environments than males, and the prediction models may be improved if the effect of gender is investigated with extended sample sizes of males and females. Similarly, the effect of age on model predictions was not investigated in this study due to limitations on recruiting old and middle-aged subjects during the pandemic. These two issues should be tested with more subjects in the future.

(4) Since the human subject tests were conducted in two locations (a carport and an environmental chamber, due to the pandemic), unexpected errors may exist in the models.

(5) Although infrared thermography can detect an occupant thermal state, an important question which we do not address here is how to control HVAC systems according to the different thermal states of multiple occupants in one room. The current study does not provide an answer to this question, but other studies offer clues about adjusting indoor temperatures according to the proportions of occupants who have non-neutral thermal states [7,

9, 40]. Future work should explore balancing different comfort demands and energy consequences in shared spaces through automatic control with thermography.

(6) Only Random Forest models were used in this study. One might also use other types of machine learning models to create models from the data, and compare the results.

(7) Existing studies on local thermal comfort (like references [15], [16], and [17]) demonstrate that occupant thermal state is affected by any local body parts that have obvious cool or warm feelings, not limited to certain body areas. While, this study demonstrates that using skin temperatures of a few fixed body parts (cheeks, nose, and hands) is sufficient to predict occupant thermal state. This study's finding is not contradictory to that of existing studies on local thermal comfort, because this study was conducted in relatively uniform thermal environments where local body parts that are easy to be cool or warm usually have similar local thermal states [41]. For example, when feet are cool and have low skin temperature, hands are also cool with low skin temperature; thus although the occupant cool state is more decided by the cool feet, the simultaneous cool hands can be used to predict occupant thermal state [42]. Nonetheless, if local heating or cooling is applied, these sensitive local body parts may have different local thermal states (e.g., locally cooling or heating feet may not affect the skin temperature of nose), and detecting fixed body parts (like cheeks and nose) may be insufficient to accurately predict occupant thermal state, which should be further investigated in the future.

6. Conclusions

This study proposes an approach to detect occupant thermal state by combining infrared thermography, computer vision technology, and machine learning models. Random Forest models were deployed to predict occupant thermal state using statistical facial and hand temperatures obtained by a TIR camera. The models have high prediction accuracy in predicting subjects' thermal sensations when using temperature data from this study. These models were also validated with the data from a separate field study [4] and lab study [36] involving larger number of subjects. We share the following conclusions:

(1) Cheek temperatures varied less with thermal sensations than nose and hand temperatures. When warm, skin temperature differences within one body region are much smaller than when neutral or cool; this is especially obvious for nose and hand. For example, the maximum cheek temperatures were 30-35, 32-36, and 35-37 °C (spans 5, 4, and 2 °C) when the subjects were cool, neutral, and warm, respectively; the corresponding nose temperatures were 22-30, 30-36, and 35-37 °C (spans 8, 6, and 2 °C), respectively; the corresponding maximum hand temperatures were 18-30, 30-36, and 35-37 °C (spans 12, 6, and 2 °C), respectively. The different responses of the cheek, nose, and hand to the ambient environments make it possible to predict the occupant thermal state using either the absolute temperatures or temperature differences of different body segments.

(2) The feature importance analysis indicated that the most important temperature variable for predicting thermal states is the cheek temperature, then the hand temperature, and not far behind, the nose temperature.

(3) Combining cheek and hand temperatures statistics with the nose temperature is sufficient to precisely predict occupant thermal state. When using the maximum or median *cheek* temperature and *nose* temperature to predict thermal states, the model accuracy is 91.9-96.3%; similarly, when using the maximum or median temperatures of *cheeks* and *hands* as inputs, the model accuracy is 93-95%. While some past studies required skin temperatures from many body locations (e.g. [23]), the models of this study only need skin temperatures from two or three body parts, which reduces the measurement difficulties compared to previous studies.

(4) Thermal state can also be predicted from intra-segment and inter-segment temperature *differences*. Using intra-segment temperature differences (cheek or hand temperature differences) provides accuracy around 70%. Using inter-segment temperature differences (temperature differences between cheek and nose and between cheek and hand) raises the model accuracy to around 80%. Combining intra- and inter-segment temperature differences simultaneously yields accuracy up to 96%. Compared to previous studies, the temperature differences approach reduces the sensitivity of measurements to TIR camera drift, increasing the prediction accuracy for lower-cost TIR cameras.

(5) Including hand temperatures in temperature difference metrics can boost model performance noticeably. When intra-segment and inter-segment temperature differences from only cheeks and noses are used (Model 13), the model prediction accuracy reached 83%. When intra-segment temperature difference from hands (maximum and median of hand skin temperatures) is also added (Model 16), the model accuracy reached 96%. Compared with previous studies, the various models using different local body parts as developed in this study allow a more flexible approach to determining occupant thermal states, especially when it is impossible to predict which body parts will be viewable by the camera.

(6) The models obtained in this study were validated by data from two independent field and lab studies with many more subjects. The prediction accuracy when applied to these studies is around 70%, which demonstrates the feasibility and applicability of the proposed models.

guidance.

Conflict of interest

The authors declare that they have no competing interests.

Author contributions

Yingdong He involved in investigation (equal); formal analysis (lead); software (supporting); visualization (lead); writing-original draft (lead); writing-review and editing (supporting).

Hui Zhang involved in conceptualization (equal); funding acquisition (lead); investigation (equal); resources (equal); writing-review and editing (equal).

Edward Arens involved in conceptualization (equal); investigation (supporting); writing-review and editing (equal); resources (supporting).

Alexander Merritt involved in formal analysis (supporting); software (equal).

Charlie Huizenga involved in formal analysis (supporting); writing-review and editing (supporting).

Ronnen Levinson involved in funding acquisition (lead); writing-review and editing (equal).

Andy Wang involved in formal analysis (supporting); software (equal).

Ali Ghahramani involved in formal analysis (supporting); software (equal).

Ana Alvarez-Suarez involved in investigation (supporting); software (supporting).

References

[1] R. Elnaklah, D. Fosas, S. Natarajan, Indoor environment quality and work performance in "green" office buildings in the Middle East, in: Building Simulation, Springer, 2020, pp. 1043-1062.

[2] J. Tang, Y. Liu, H. Du, L. Lan, Y. Sun, J. Wu, The effects of portable cooling systems on thermal comfort and work performance in a hot environment, in: Building Simulation, Springer, 2021, pp. 1667-1683.

[3] ANSI/ASHRAE, ASHRAE Standard 55-2020: Thermal environmental conditions for human occupancy, American Society of Heating, Refrigerating and Air-Conditioning Engineering, Atlanta, GA, (2020).

[4] J. Hu, Y. He, X. Hao, N. Li, Y. Su, H. Qu, Optimal temperature ranges considering gender differences in thermal comfort, work performance, and sick building syndrome: A winter field study in university classrooms, Energy and Buildings, 254 (2022) 111554.

[5] Z. Wang, H. Zhang, Y. He, M. Luo, Z. Li, T. Hong, B. Lin, Revisiting individual and group differences in thermal comfort based on ASHRAE database, Energy and Buildings, (2020) 110017.

[6] Y. He, N. Li, J. Peng, W. Zhang, Y. Li, Field study on adaptive comfort in air conditioned dormitories of university with hot-humid climate in summer, Energy and Buildings, 119 (2016) 1-12.

[7] Y. He, N. Li, J. Lu, N. Li, Q. Deng, C. Tan, J. Yan, Meeting thermal needs of occupants in shared space with an adjustable thermostat and local heating in winter: An experimental study, Energy and Buildings, 236 (2021) 110776.

[8] Y. He, T. Parkinson, E. Arens, H. Zhang, N. Li, J. Peng, J. Elson, C. Maranville, Creating alliesthesia in cool

environments using personal comfort systems, Building and Environment, 209 (2021) 108642.

[9] Y. He, N. Li, H. Zhang, Y. Han, J. Lu, L. Zhou, Air-conditioning use behaviors when elevated air movement is available, Energy and Buildings, (2020) 110370.

[10] G. Paliaga, H. Zhang, T. Hoyt, E. Arens, Eliminating Overcooling Discomfort While Saving Energy: A Surprisingly Straightforward Solution, ASHRAE Journal, 61 (4) (2019) 14-24.

[11] E. Arens, H. Zhang, T. Hoyt, S. Kaam, F. Bauman, Y. Zhai, G. Paliaga, J. Stein, R. Seidl, B. Tully, Effects of diffuser airflow minima on occupant comfort, air mixing, and building energy use (RP-1515), Science and Technology for the Built Environment, 21 (8) (2015) 1075-1090.

[12] M. Mendell, A. Mirer, Indoor thermal factors and symptoms in office workers: findings from the US EPA BASE study, in, Lawrence Berkeley National Lab.(LBNL), Berkeley, CA (United States), 2008.

[13] X. Cheng, B. Yang, A. Hedman, T. Olofsson, H. Li, L. Van Gool, NIDL: A pilot study of contactless measurement of skin temperature for intelligent building, Energy and Buildings, 198 (2019) 340-352.

[14] B. Yang, X. Cheng, D. Dai, T. Olofsson, H. Li, A. Meier, Real-time and contactless measurements of thermal discomfort based on human poses for energy efficient control of buildings, Building and Environment, 162 (2019) 106284.

[15] H. Zhang, E. Arens, C. Huizenga, T. Han, Thermal sensation and comfort models for non-uniform and transient environments: Part I: Local sensation of individual body parts, Building and Environment, 45 (2) (2010) 380-388.

[16] H. Zhang, E. Arens, C. Huizenga, T. Han, Thermal sensation and comfort models for non-uniform and transient environments, part II: Local comfort of individual body parts, Building and Environment, 45 (2) (2010) 389-398.

[17] H. Zhang, E. Arens, C. Huizenga, T. Han, Thermal sensation and comfort models for non-uniform and transient environments, part III: Whole-body sensation and comfort, Building and Environment, 45 (2) (2010) 399-410.

[18] B. Yang, X. Li, Y. Hou, A. Meier, X. Cheng, J.-H. Choi, F. Wang, H. Wang, A. Wagner, D. Yan, Non-invasive (non-contact) measurements of human thermal physiology signals and thermal comfort/discomfort poses-a review, Energy and Buildings, 224 (2020) 110261.

[19] F. De Oliveira, S. Moreau, C. Gehin, A. Dittmar, Infrared imaging analysis for thermal comfort assessment, in: 2007 29th Annual international conference of the IEEE engineering in medicine and biology society, IEEE, 2007, pp. 3373-3376.

[20] A. Ghahramani, G. Castro, B. Becerik-Gerber, X. Yu, Infrared thermography of human face for monitoring thermoregulation performance and estimating personal thermal comfort, Building and Environment, 109 (2016) 1-11.

[21] F. Wang, B. Zhu, R. Li, D. Han, Z. Sun, S. Moon, Z. Gong, W. Yu, Smart control of indoor thermal environment based on online learned thermal comfort model using infrared thermal imaging, in: 2017 13th IEEE Conference on Automation Science and Engineering (CASE), IEEE, 2017, pp. 924-925.

[22] F. Faridah, M.M. Waruwu, T. Wijayanto, R. Budiarto, R.C. Pratama, S.E. Prayogi, N.M. Nadiya, R.J. Yanti, Feasibility study to detect occupant thermal sensation using a low-cost thermal camera for indoor environments in Indonesia, Building Services Engineering Research and Technology, (2021) 0143624421994015.

[23] D. Li, C.C. Menassa, V.R. Kamat, Non-intrusive interpretation of human thermal comfort through analysis of facial infrared thermography, Energy and Buildings, 176 (2018) 246-261.

[24] X. Li, Q. Chen, Development of a novel method to detect clothing level and facial skin temperature for controlling HVAC systems, Energy and Buildings, 239 (2021) 110859.

[25] A.C. Cosma, R. Simha, Thermal comfort modeling in transient conditions using real-time local body temperature extraction with a thermographic camera, Building and Environment, 143 (2018) 36-47.

[26] B. Tejedor, M. Casals, M. Gangolells, M. Macarulla, N. Forcada, Human comfort modelling for elderly people by infrared thermography: Evaluating the thermoregulation system responses in an indoor environment during winter, Building and Environment, 186 (2020) 107354.

[27] A. Ghahramani, Q. Xu, S. Min, A. Wang, H. Zhang, Y. He, A. Merritt, R. Levinson, Infrared-Fused Vision-Based Thermoregulation Performance Estimation for Personal Thermal Comfort-Driven HVAC System Controls, Buildings, 12

(8) (2022) 1241.

[28] H. Yoshikawa, A. Uchiyama, T. Higashino, ThermalWrist: Smartphone Thermal Camera Correction Using a Wristband Sensor, Sensors, 19 (18) (2019) 3826.

[29] Blackfly S GigE, 2021, https://www.flir.com/products/blackfly-s-gige/?creative=497995702464&keyword=bfs-pge-50s5c-c&matchtype=e&network=g&device=c&gclid=CjwKCAjw8KmLBhB8EiwAQbqNoD7u9Cs5zkerGpVgPrrvPRFed79pVVpVMMeQFOdGgh3IIVJ3oOLJHRoCWhAQAvD_BwE

[30] FLIR A315 IR Temperature Sensor with GigE (Motorized Focus), 2021, https://www.flir.com/products/a315/

[31] Z. Cao, G. Hidalgo, T. Simon, S.-E. Wei, Y. Sheikh, OpenPose: realtime multi-person 2D pose estimation using Part Affinity Fields, IEEE transactions on pattern analysis and machine intelligence, 43 (1) (2019) 172-186.

[32] G. Bradski, The openCV library, Dr. Dobb's Journal: Software Tools for the Professional Programmer, 25 (11) (2000) 120-123.

[33] N.V. Chawla, K.W. Bowyer, L.O. Hall, W.P. Kegelmeyer, SMOTE: synthetic minority over-sampling technique, Journal of artificial intelligence research, 16 (2002) 321-357.

[34] L. Breiman, A. Cutler, Random Forests, 2006, https://www.stat.berkeley.edu/~breiman/RandomForests/cc_home.htm

[35] F. Pedregosa, G. Varoquaux, A. Gramfort, V. Michel, B. Thirion, O. Grisel, M. Blondel, P. Prettenhofer, R. Weiss, V. Dubourg, Scikit-learn: Machine learning in Python, the Journal of machine Learning research, 12 (2011) 2825-2830.

[36] H. Zhang, Human thermal sensation and comfort in transient and non-uniform thermal environments, Ph.D thesis, University of California, Berkeley, 2003.

[37] C. Dai, H. Zhang, E. Arens, Z. Lian, Machine learning approaches to predict thermal demands using skin temperatures: Steady-state conditions, Building and Environment, 114 (2017) 1-10.

[38] R. Olbrycht, B. Więcek, G. De Mey, Thermal drift compensation method for microbolometer thermal cameras, Applied Optics, 51 (11) (2012) 1788-1794.

[39] P.W. Nugent, J.A. Shaw, N.J. Pust, Correcting for focal-plane-array temperature dependence in microbolometer infrared cameras lacking thermal stabilization, Optical Engineering, 52 (6) (2013) 061304.

[40] Y. He, N. Li, N. Li, J. Li, J. Yan, C. Tan, Control behaviors and thermal comfort in a shared room with desk fans and adjustable thermostat, Building and Environment, 136 (2018) 213-226.

[41] Y. He, N. Li, M. He, D. He, Using radiant cooling desk for maintaining comfort in hot environment, Energy and Buildings, 145 (2017) 144-154.

[42] Y. He, X. Wang, N. Li, M. He, D. He, Heating chair assisted by leg-warmer: A potential way to achieve better thermal comfort and greater energy conservation in winter, Energy and Buildings, 158 (2018) 1106-1116.